PHILOSOPHICAL TRANSACTIONS OF THE ROYAL SOCIETY A MATHEMATICAL, PHYSICAL & ENGINEERING SCIENCES

Simulation of three–pulse–echo and fluorescence depolarization in photosynthetic aggregates

Wei Min Zhang, Torsten Meier, Vladimir Chernyak and Shaul Mukamel

Phil. Trans. R. Soc. Lond. A 1998 **356**, 405-419
doi: 10.1098/rsta.1998.0173

The Royal Society

Simulation of three-pulse-echo and fluorescence depolarization in photosynthetic aggregates

By Wei Min Zhang, Torsten Meier, Vladimir Chernyak and Shaul Mukamel

Department of Chemistry and Rochester Theory Center for Optical Science and Engineering, University of Rochester, Rochester, NY 14627, USA

Femtosecond spectroscopies of chlorophyll dimers and the LH2 antenna complex are calculated using a theory that incorporates the effects of two-exciton states, static disorder and coupling of excitons to phonons with an arbitrary spectral density. Applications are made to pump-probe and echo peak-shift measurements in the B820 dimers, and to fluorescence depolarization in the B850 system of the LH2 antenna of purple bacteria.

Keywords: LH2 antenna; B820 dimer; exciton transport; photon echo; pump probe; depolarization

1. Introduction

Energy and charge transfer processes in light harvesting systems have been the subject of intensive experimental and theoretical studies (Grondelle *et al.* 1994; Sundström & Grondelle 1995; McDermott *et al.* 1995). Special attention has been given recently to the LH2 antenna complexes in purple bacteria (McDermott *et al.* 1995), following the determination of their structure (McDermott *et al.* 1995; Hu & Schulten 1997; Hoff & Deisenhofer 1997). LH1 has a single absorption band with a maximum at about 880 nm (B880), while the peripheral antenna LH2 has two distinct absorption maxima at 800 nm (B800) and 850 nm (B850) (Pullerits & Sundström 1996). Circular dichroism measurements suggest that the B800 band is due to the absorption by monomeric BChl a (bacteriochlorophyll) molecules, whereas the B850 band originates from exciton-coupled BChl molecules. The 2.5 Å resolution crystal structure of LH2 of *Rhodopseudomonas* (Rps.) shows 27 Bchl a monomers arranged in two rings (McDermott *et al.* 1995). Nine of the Bchl a molecules with planes parallel to the membrane plane form an outer ring while the other eighteen molecules with planes perpendicular to the membrane plane form an inner ring (McDermott *et al.* 1995). LH1 has a similar but larger ring of 32 BChl a molecules. There are strong indications suggesting that the pigments of LH1 can be described as an assembly of 16 Bchl dimers. The dimer is the smallest pigment-proteins complex, consisting of two short polypeptides and two BChl a molecules (Karrasch *et al.* 1995) and has an absorption maximum at 820 nm. When subjected to the right environment (detergent micelle), LH1 can be reversibly dissociated into its B820 units. The similarities of triplet-minus-singlet (T–S) and excited state difference spectra between LH1 and the dimer indicate that the dimeric nature of B820 is maintained in the fully assem-

bled LH1. The transition dipoles in the dimer are organized in a head–tail orientation with an angle of less than 20° between the dipoles (Koolhaas *et al.* 1994).

The interpretation of linear and nonlinear spectroscopic measurements in these complexes constitutes a complicated task because of strong coupling of electronic degrees of freedom to intramolecular, intermolecular and solvent nuclear motions (exciton–phonon coupling). Intermolecular interactions lead to the formation of delocalized electronic excitations and strong energetic disorder tends to localize these excitations. Existing theories of optical response in molecular aggregates employ the Frenkel exciton Hamiltonian which describes an assembly of interacting two- or three-level molecules. As outlined in Meier *et al.* (1997*a*), these theories can be classified according to the level of reduction with respect to nuclear motions. The simplest approach is based on the complete elimination of nuclear degrees of freedom, taking them into account through relaxation superoperators. This approach has been recently applied to interpret pump-probe time-resolved fluorescence and superradiance signals in LH2 antenna complexes (Meier *et al.* 1997*b*). In Meier *et al.* (1997*c*), superradiance of LH2 has been calculated, taking into account polaron effects originating from strong exciton–phonon coupling by invoking different *ansätze* for the polaron wave functions. The theories of Meier *et al.* (1997*a*,*b*) did not follow the time evolution of exciton or polaron populations but focused on the signals in the long-time limit. Two-pulse photon echoes have been calculated in Meier *et al.* (1997*a*) using a different approach which included diagonal exciton–phonon coupling explicitly but completely neglected phonon-induced coupling between different excitons.

In this paper we extend the theory of Meier *et al.* (1997*a*) to general (three-pulse) time-domain four-wave mixing techniques. The present approach is based on neglecting off-diagonal exciton–phonon coupling on time intervals where exciton coherences are involved, whereas evolution of exciton populations is calculated by treating the off-diagonal coupling perturbatively via relaxation superoperators for populations of polarons (i.e. excitons dressed by phonons). Our approach holds when effects of exciton localization due to static disorder are stronger than phonon-induced self-trapping. It takes into account the distortions of nuclear positions due to the localized form of the exciton wave function originating from static disorder, and neglects the influence of these distortions on the shape of the exciton wave function. The present theory provides a unified description of different optical signals, which is an important step towards the determination of dynamic interaction parameters in light-harvesting complexes.

The theory is outlined in § 2. Applications to three-pulse echo and pump-probe signals in chlorophyll dimers are presented in § 3. In § 4 we calculate the depolarization signal in LH2 and compare with recent experiments. Finally, we summarize our results in § 5.

2. Nonlinear optical response of Frenkel excitons coupled to a phonon bath

We employ a Frenkel-exciton model of an aggregate made of N two-level molecules coupled to a nuclear bath. The Hamiltonian is given by

$$H = \sum_n \Omega_n(\boldsymbol{q}) \bar{B}_n^\dagger \bar{B}_n + \sum_{mn}^{m\neq n} J_{mn}(\boldsymbol{q}) \bar{B}_m^\dagger \bar{B}_n + H_{\mathrm{ph}}, \tag{2.1}$$

where $\bar{B}_n$ ($\bar{B}_n^\dagger$) are exciton annihilation (creation) operators on the nth molecule, with commutation relations

$$[\bar{B}_m, \bar{B}_n^\dagger] = \delta_{mn}(1 - 2\bar{B}_m^\dagger \bar{B}_m), \tag{2.2}$$

$H_{\rm ph}$ is the phonon Hamiltonian and $\boldsymbol{q}$ represents the complete set of nuclear coordinates. $\Omega_n(\boldsymbol{q})$ is the transition frequency of molecule n and $J_{mn}(\boldsymbol{q})$ is the dipole–dipole interaction matrix element between molecules n and m. Exciton–phonon coupling is incorporated through the $\boldsymbol{q}$ dependence of Ω_n and J_{mn}. The polarization operator P representing coupling of the aggregate to the optical field $-E(t)\cdot P$ has the form

$$P = \sum_n d_n(\bar{B}_n^\dagger + \bar{B}_n). \tag{2.3}$$

This Hamiltonian conserves the number of electronic excitations, and its eigenstates separate into bands of states with a fixed number of excited molecules. The third-order spectroscopies discussed in this paper only involve the ground state $|0\rangle$, the one exciton $|\mu\rangle$ and two-exciton $|\bar{\mu}\rangle$ bands (figure 1). Transforming the operators to the exciton representation yields

$$\left.\begin{aligned} B_\mu^\dagger|0\rangle &\equiv \sum_n \varphi_\mu(n)\bar{B}_n^\dagger|0\rangle, \quad B_\mu^\dagger \bar{B}_m^\dagger|0\rangle = 0, \\ Y_{\bar{\mu}}^\dagger|0\rangle &\equiv \sum_{mn} \Psi_{\bar{\mu}}(m,n)\bar{B}_m^\dagger \bar{B}_n^\dagger|0\rangle, \quad Y_{\bar{\mu}}^\dagger \bar{B}_m^\dagger|0\rangle = 0, \end{aligned}\right\} \tag{2.4}$$

where $|0\rangle$ is the ground state of the electronic system. $\varphi_\mu(n)$ and $\Psi_{\bar{\mu}}(m,n)$ represent the one- and two-exciton eigenstates of the exciton Hamiltonian with energies ϵ_μ and $\epsilon_{\bar{\mu}}$, respectively. It follows from equation (2.4) that $B_\mu^\dagger B_\nu^\dagger|0\rangle = 0$, which implies that two-exciton states are obtained from the ground state by means of two-exciton creation operators $Y_{\bar{\mu}}^\dagger$ rather than by bilinear combinations of one-exciton creation operators. The one- and two-exciton operators are defined such that B_μ and $B_\mu^\dagger$ have non-zero matrix elements between the ground and one-exciton states, whereas $Y_{\bar{\mu}}$ and $Y_{\bar{\mu}}^\dagger$ have non-zero matrix elements between the ground and two-exciton states only. Operators which create two-exciton states by acting on one-exciton states are represented by $Y_{\bar{\mu}}^\dagger B_\mu$ (see figure 1). Using these operators, the Hamiltonian assumes the form

$$H = H_0 + H_1, \tag{2.5}$$

with

$$H_0 \equiv \sum_\mu \epsilon_\mu B_\mu^\dagger B_\mu + \sum_{\bar{\mu}} \epsilon_{\bar{\mu}} Y_{\bar{\mu}}^\dagger Y_{\bar{\mu}} + \sum_\mu q_\mu^{(\rm c)} B_\mu^\dagger B_\mu + \sum_{\bar{\mu}} q_{\bar{\mu}}^{(\rm c)} Y_{\bar{\mu}}^\dagger Y_{\bar{\mu}} + H_{\rm ph}$$

and

$$H_1 \equiv \sum_{\mu\nu}^{\mu\neq\nu} q_{\mu\nu}^{(\rm c)} B_\mu^\dagger B_\nu + \sum_{\bar{\mu}\bar{\nu}}^{\bar{\mu}\neq\bar{\nu}} q_{\bar{\mu}\bar{\nu}}^{(\rm c)} Y_{\bar{\mu}}^\dagger Y_{\bar{\nu}}. \tag{2.6}$$

The polarization operator is given by

$$P = \sum_\mu d_\mu(B_\mu + B_\mu^\dagger) + \sum_{\mu\bar{\mu}} d_{\mu,\bar{\mu}}(Y_{\bar{\mu}}^\dagger B_\mu + B_\mu^\dagger Y_{\bar{\mu}}), \tag{2.7}$$

with

$$d_\mu = \sum_m d_m \varphi_\mu(m), \quad d_{\mu,\bar{\mu}} = \sum_{mn} \Psi_{\bar{\mu}}[\varphi_\mu(m)d_n + \varphi_\mu(n)d_m]. \tag{2.8}$$

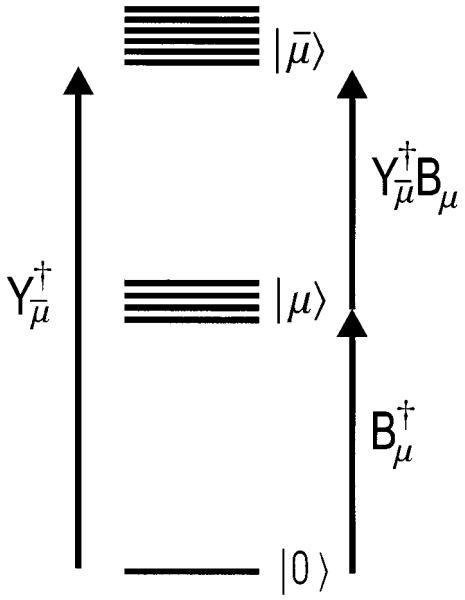

Figure 1. Exciton level structure and transition dipoles of an aggregate made out of an N interacting two-level molecules. $|0\rangle$ is the ground state, $|\mu\rangle$ is the single exciton band and $|\bar{\mu}\rangle$ is the two-exciton band. The operators inducing transitions between bands are displayed as well.

$q^{(c)}$ are collective nuclear coordinate which couple to the various electronic varibles. In circular one-dimensional aggregates with nearest-neighbour exciton coupling, the many-exciton states are represented by the Bethe ansatz (Zhang *et al.* 1998; Baxter 1982) and can be expressed in terms of two sets of one-exciton states: ordinary one-exciton states $\varphi_{\mu}(n)$ satisfying periodic boundary conditions $\varphi_{\mu}(n+N) = \varphi_{\mu}(n)$, and auxiliary one-exciton states $\bar{\varphi}_{\mu}(n)$ with antiperiodic boundary conditions $\bar{\varphi}_{\mu}(n+N) = -\bar{\varphi}_{\mu}(n)$, both being eigenstates of the one-exciton Hamiltonian with energies ϵ_{μ} and $\bar{\epsilon}_{\mu}$, respectively. For the LH1 complex (B880), its B820 dimer and the B850 and B800 system of LH2 we have $N = 32$, 2, 18 and 9, respectively.

The phonon Hamiltonian H_{ph} is assumed to represent a continuous distribution of harmonic degrees of freedom. We further assume that each molecule has its own bath and that baths belonging to different molecules are uncorrelated. In this case, all relevant information about nuclear dynamics is contained in the spectral density $C(\omega)$. The spectral broadening function $g(t)$ is given by (Mukamel 1995)

$$g(t) = -\frac{1}{2\pi}\int_{-\infty}^{\infty}\frac{\mathrm{d}\omega}{\omega^2}\,C(\omega)[1+\coth(\tfrac{1}{2}\beta\hbar\omega)][\exp(-\mathrm{i}\omega t)+\mathrm{i}\omega t-1]. \tag{2.9}$$

The real part of $g(t)$ describes the decay of optical excitations, whereas the imaginary part represents the Stokes shift.

The time-domain optical response function $\hat{R}(t_3,t_2,t_1)$, which relates the third-order nonlinear polarization $P^{(3)}(t)$ to the driving field $E(t)$, is defined by (assuming that pulse 1 comes first, then pulse 2 and pulse 3 is the last) (Mukamel 1995)

$$P^{(3)}(t) = i^3\int_0^{\infty}\mathrm{d}t_3\int_0^{\infty}\mathrm{d}t_2\int_0^{\infty}\mathrm{d}t_1\,\hat{R}(t_3,t_2,t_1)E_3(t-t_3)E_2(t-t_3-t_2)E_1(t-t_3-t_2-t_1). \tag{2.10}$$

The response function $\hat{R}(t_3,t_2,t_1)$ has been calculated using projection operator

techniques (Zwanzig 1961, 1964; Mori 1965*a*,*b*). The projection is defined for exciton population wavepackets and includes nuclear reorganization due to diagonal exciton–phonon coupling. After some algebra, we recast $\hat{R}$ in the doorway-windows (DW) representation (Zhang *et al.* 1998)

$$\hat{R}(t_3,t_2,t_1)=\sum_{\mu\nu}W_\mu(t_3)G_{\mu\nu}(t_2)D_\nu(t_1)+\sum_{\mu\nu}D_\mu(t_3)D_\nu(t_1)+R^{(\mathrm{s})}(t_3,t_2,t_1). \quad (2.11)$$

The first term may be interpreted as follows. The doorway function $D_\nu(t_1)$ describes the population of the νth exciton after two interactions with the driving field, separated by the time interval t_1. $G_{\mu\nu}(t_2)$ is the Green function of the generalized master equation describing the dynamics of polaron populations during the time interval t_2. Finally, the window function $W_\mu(t_3)$ represents the time evolution during the third time interval. The second term in equation (2.11) is the bleaching contribution (adopting the terminology of pump-probe spectroscopy); $\sum_\nu D_\nu(t_1)$ represents the total exciton population induced by two interactions with the driving field and $D_\mu(t_3)$ represents the window function which in the bleaching case coincides with the doorway function. Finally, the third term $R^{(\mathrm{s})}$ is the short-time component which vanishes at $t_2\rightarrow\infty$. Using the exciton representation, the doorway and window functions can be written as

$$D_\nu(t_1)=\sum_\nu(\boldsymbol{e}_2\cdot\boldsymbol{d}_\nu)(\boldsymbol{e}_1^*\cdot\boldsymbol{d}_\nu)\exp[\mathrm{i}\epsilon_\nu t_1-g^*_{\nu\nu}(t_1)], \quad (2.12)$$

$$D_\mu(t_3)=\sum_\mu(\boldsymbol{e}_s\cdot\boldsymbol{d}_\mu)(\boldsymbol{e}_3\cdot\boldsymbol{d}_\mu)\exp[-\mathrm{i}\epsilon_\mu t_3-g_{\mu\mu}(t_3)], \quad (2.13)$$

$$\begin{aligned}W_\mu(t_3)=&(\boldsymbol{e}_s\cdot\boldsymbol{d}_\mu)(\boldsymbol{e}_3\cdot\boldsymbol{d}_\mu)\exp[-\mathrm{i}\epsilon_\mu t_3-g^*_{\mu\mu}(t_3)-2\mathrm{i}\lambda_{\mu\mu}t_3]\\&-\sum_{\bar\nu}(\boldsymbol{e}_s\cdot\boldsymbol{d}_{\mu,\bar\nu})(\boldsymbol{e}_3\cdot\boldsymbol{d}_{\mu,\bar\nu})\exp[-\mathrm{i}(\epsilon_{\bar\nu}-\epsilon_\mu)t_3]\\&\times\exp[-g_{\mu\mu}(t_3)-g_{\bar\nu\bar\nu}(t_3)+2g_{\mu\bar\nu}(t_3)+2\mathrm{i}(\lambda_{\mu\bar\nu}-\lambda_{\mu\mu})t_3]. \quad (2.14)\end{aligned}$$

In these equations $\lambda_{\mu\nu}$ and $g_{\mu\nu}$ are the abbreviated notation for $\lambda_{\mu\mu,\nu\nu}$ and $g_{\mu\mu,\nu\nu}$, defined as

$$\lambda_{\mu\nu,\mu'\nu'}\equiv-\lim_{\tau\rightarrow\infty}\mathrm{Im}\left[\frac{\mathrm{d}g_{\mu\nu,\mu'\nu'}(\tau)}{\mathrm{d}\tau}\right], \quad (2.15)$$

$$g_{\mu\nu,\mu'\nu'}(t)=g(t)\sum_n\varphi_\mu(n)\varphi_\nu(n)\varphi_{\mu'}(n)\varphi_{\nu'}(n). \quad (2.16)$$

Note that the window (equation (2.14)) has two terms representing the contribution of the μth polaron population to the signal. The first involves transition down to the ground state and the second involves the two exciton states. In pump-probe spectroscopy they are responsible for stimulated emission and excited state absorption, respectively. This will be discussed in the next section.

Assuming fast nuclear relaxation coupled with exciton transport, the Green function satisfies the Master equation (for $t>0$),

$$\frac{\mathrm{d}}{\mathrm{d}t}G_{\mu\nu}(t)-\sum_\alpha^{\alpha\neq\mu}[K_{\mu\alpha}G_{\alpha\nu}(t)-K_{\alpha\nu}G_{\mu\nu}(t)]=\delta_{\mu\nu}\delta(t), \quad (2.17)$$

with the initial condition $G_{\mu\nu}(0)=\delta_{\mu\nu}$. A straightforward calculation of the relax-

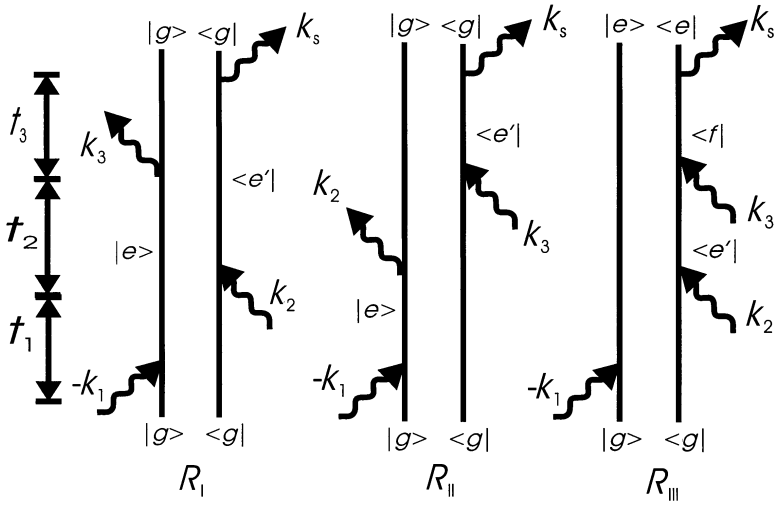

Figure 2. Double-sided Feynman diagrams representing the three contributions to the time-domain four-wave mixing signal at $\boldsymbol{k}_3 + \boldsymbol{k}_2 - \boldsymbol{k}_1$ which survive the rotating wave approximation.

ation kernel to second order in H_1 yields

$$K_{\mu\nu} \equiv \int_0^\infty 2\,\mathrm{Re}[K^{\mathrm{L}}_{\mu\nu}(t)]\,\mathrm{d}t, \tag{2.18}$$

where

$$\begin{aligned} K^{\mathrm{L}}_{\mu\nu}(t) = \{&\ddot{g}_{\mu\nu,\nu\mu}(t) - [\dot{g}_{\nu\mu,\nu\nu}(t) - \dot{g}_{\nu\mu,\mu\mu}(t) + 2\mathrm{i}\lambda_{\nu\mu,\nu\nu}] \\ &\times [\dot{g}_{\nu\nu,\mu\nu}(t) - \dot{g}_{\mu\mu,\mu\nu}(t) + 2\mathrm{i}\lambda_{\mu\nu,\nu\nu}]\} \exp[-\mathrm{i}(\epsilon_\mu - \epsilon_\nu)t] \\ &\times \exp\{-[g_{\mu\mu,\mu\mu}(t) + g_{\nu\nu,\nu\nu}(t) - g_{\nu\nu,\mu\mu}(t) - g_{\mu\mu,\nu\nu}(t) \\ &+2\mathrm{i}(\lambda_{\nu\nu,\nu\nu} - \lambda_{\mu\mu,\nu\nu})t]\}. \end{aligned} \tag{2.19}$$

The short-time component $R^{(\mathrm{s})}$ is given by

$$R^{(\mathrm{s})}(t_3, t_2, t_1) = R(t_3, t_2, t_1) - R(t_3, \infty, t_1), \tag{2.20}$$

with

$$R(t_3, t_2, t_1) = \sum_{\alpha=1}^{4} \sum_{j=1}^{2} [R_{\alpha j}(t_3, t_2, t_1) - R^*_{\alpha j}(t_3, t_2, t_1)]. \tag{2.21}$$

For the present three-electronic-band system (ground state, one exciton and two-exciton) only three out of the sixteen contributions to $R(t_3, t_2, t_1)$ survive when invoking the rotating wave approximation. The double-side Feynman diagrams of these terms R_{I}, R_{II} and R_{III} are shown in figure 2 and explicit expressions are given in Appendix A.

The second term in equation (2.20) can be recast in a form

$$R(t_3, \infty, t_1) = \sum_{\nu} W_\nu(t_3) D_\nu(t_1) + \sum_{\mu\nu} D_\mu(t_3) D_\nu(t_1), \tag{2.22}$$

where the first term is equal to the first term of equation (2.11) with $G_{\mu\nu}(0) \equiv \delta_{\mu\nu}$, whereas the second term coincides with the bleaching contribution.

Disorder is incorporated by implementing a Monte-Carlo averaging over a Gaussian distribution of molecular frequencies which are assumed to be uncorrelated

$$f_1(\Omega_n) = \frac{1}{\sqrt{2\pi}\sigma} \exp\left(\frac{-(\Omega_n - \bar{\Omega}_n)^2}{2\sigma^2}\right), \tag{2.23}$$

where Ω_n is the optical transition frequency of the nth molecule.

3. Application to chlorophyll dimers

In the following simulations of the B820 system we employ a simple model of the bath assuming the spectral density of an overdamped Brownian oscillator (Mukamel 1995),

$$C(\omega) = 2\lambda \frac{\omega\tau_1}{\omega^2\tau_1^2 + 1}, \tag{3.1}$$

with the same parameters for all molecules. The reorganization-energy parameter λ denotes the exciton–phonon coupling strength, whereas τ_1 is the relaxation timescale of the collective coordinate. For this model, the correlation function of the electronic energy gap adopts the form

$$M(t) \equiv \langle q^{(c)}(t) q^{(c)}(0)\rangle = \frac{1}{\pi\lambda} \int_0^\infty \mathrm{d}\omega \, \frac{C(\omega)}{\omega} \cos(\omega t) = \mathrm{e}^{-|t|/\tau_1}. \tag{3.2}$$

In all calculations we set $\tau_1 = 130\,\mathrm{fs}$, corresponding to a nuclear relaxation rate of $\Lambda \equiv 1/\tau_1 = 256\,\mathrm{cm}^{-1}$. λ was varied in the range from 80–320 cm^{-1}. The behaviour of the overdamped Brownian oscillator depends crucially on the parameter $\kappa \equiv \Lambda/\Delta$ where $\Delta \equiv \sqrt{2\lambda k_\mathrm{B} T}$ (Mukamel 1995). The limits of $\kappa \ll 1$ and $\kappa \gg 1$ are known as the spectral diffusion (static) and the homogeneous limits, respectively. Our parameters interpolate between the two limits: for $\lambda = 80\,\mathrm{cm}^{-1}$, $\Delta = 183\,\mathrm{cm}^{-1}$ and $\kappa > 1$, whereas for $\lambda = 320\,\mathrm{cm}^{-1}$, $\Delta = 360\,\mathrm{cm}^{-1}$ and $\kappa < 1$.

The linear absorption lineshape is given by

$$S_\mathrm{a}(\omega) = \mathrm{Im} \int_0^\infty \mathrm{d}t \, \exp(\mathrm{i}\omega t) \sum_\nu \mathrm{i}|\boldsymbol{e}_1 \cdot \boldsymbol{d}_\nu|^2 \exp[-\mathrm{i}\epsilon_\nu t - g_{\nu\nu}(t)], \tag{3.3}$$

where ϵ_ν is the one-exciton energy. $|\boldsymbol{e}_1 \cdot \boldsymbol{d}_\nu|^2$ is proportional to the oscillator strength in νth exciton. In our calculations, we adjusted the value of disorder σ to fit the linear absorption linewidth (which is 630 cm^{-1} for the dimer (Yu *et al.* 1997) and 470 cm^{-1} for LH2 (Jimenez *et al.* 1997)) for each value of the exciton–phonon coupling strength λ.

(*a*) *Echo peak shift*

The time-resolved four-wave mixing signal induced by impulsive (very short) laser pulses is given by (Mukamel 1995)

$$S_0(t_3, t_2, t_1) \propto |\hat{R}(t_3, t_2, t_1)|^2. \tag{3.4}$$

The photon echo technique which detects the signal generated at $\boldsymbol{k}_3 + \boldsymbol{k}_2 - \boldsymbol{k}_1$ (see figure 2) does not always produce an echo signal. This depends on the nature of the system and the broadening mechanism (Mukamel 1995). The echo which peaks at $t_1 = t_3$ can be observed by time-resolved detection (equation (3.4)). Figure 3 shows the time resolved signal $S_0(t_3, t_2, t_1)$ (using $\lambda = 110\,\mathrm{cm}^{-1}$ and $\sigma = 270\,\mathrm{cm}^{-1}$) for

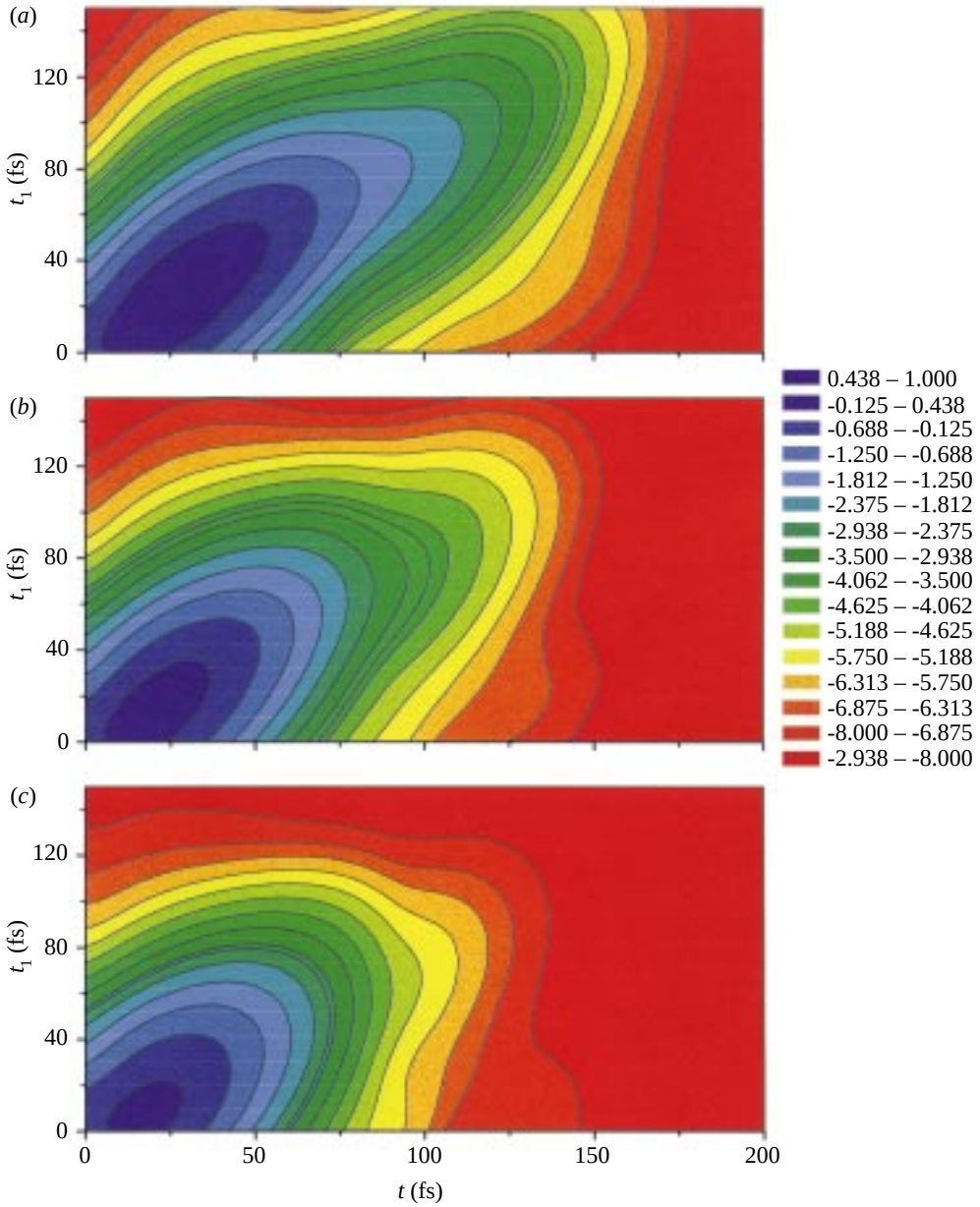

Figure 3. Contour plots of $\log[S_0(t, t_2, t_1)]$ of the B820 dimer: $\lambda = 110\ \mathrm{cm}^{-1}$; $\sigma = 270\ \mathrm{cm}^{-1}$; (*a*) $t_2 = 0$ fs; (*b*) $t_2 = 100$ fs; (*c*) $t_2 = 400$ fs.

different time intervals $t_2 = 0$, 100 and 400 fs. For $t_2 = 0$, the maximum of the time-resolved signals appear at longer time t_3 with increasing t_1. For larger t_1, the position of the maximum is close to t_1 indicating the photo-echo nature of the signal. With increasing t_2, the amplitude of the signal decreases slightly and the maximum of the time-resolved signal appears at earlier times, because population relaxation partially destroys the echo.

Characteristic signatures of the echo are contained in the simpler and more com-

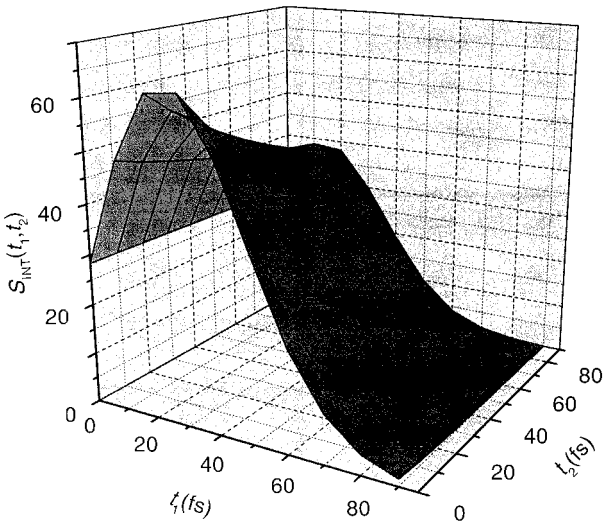

Figure 4. Integrated photon echo signal $S_{\mathrm{INT}}(t_1, t_2)$ of the B820 dimer: $\lambda = 110\ \mathrm{cm}^{-1}$; $\sigma = 270\ \mathrm{cm}^{-1}$.

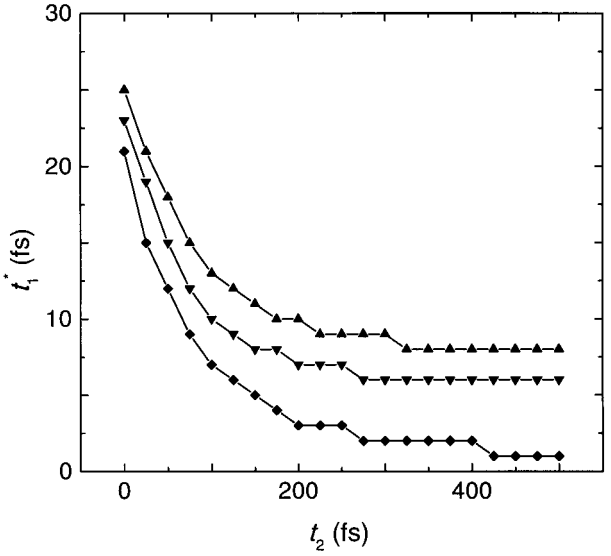

Figure 5. Peak shift of the B820 dimer. (▲) $\lambda = 110\ \mathrm{cm}^{-1}$, $\sigma = 270\ \mathrm{cm}^{-1}$; (▼) $\lambda = 150\ \mathrm{cm}^{-1}$, $\sigma = 240\ \mathrm{cm}^{-1}$; (♦) $\lambda = 320\ \mathrm{cm}^{-1}$, $\sigma = 120\ \mathrm{cm}^{-1}$.

mon integrated detection obtained by integrating equation (3.4) over the observation time t_3:

$$S_{\mathrm{INT}}(t_2, t_1) = \int_0^\infty S_0(t_3, t_2, t_1)\, \mathrm{d}t_3. \tag{3.5}$$

Figure 4 displays $S_{\mathrm{INT}}(t_2, t_1)$ for the dimer. One can see a fast decay along t_1 and a slower decay along t_2. The maximum appears at about $t_1 = 25$ fs, $t_2 = 0$. These values are related to the disorder strength and homogeneous dephasing. During the t_2 time interval, the system is maintained in polaron population states which relax to equilibrium when $t_2 \to \infty$.

The figure shows that the time-integrated signal starts with a finite value at $t_1 = 0$, reaches a maximum and then decays to zero. This behaviour comes from the fact that the system is inhomogeneously broadened. The maximum value t_1^* (denoted the peak shift) is determined by the ratio of the echo width (inhomogeneous broadening) and the homogeneous dephasing time, as well as by the time delay t_2. Measuring the peak shift may provide some valuable information about the temporal behaviour of the time-resolved signal even though a time-integrated detection is used (Yu *et al.* 1997; Jimenez *et al.* 1997; Joo *et al.* 1996; de Boeij *et al.* 1996).

The peak shift for the B820 dimer subunit of LH1 has been measured recently (Yu *et al.* 1997). It was found that its value for the dimer is much larger compared to that of the LH1 complex (Jimenez *et al.* 1997). This result was attributed to the fact that in LH1 the peak shift is destroyed by energy-transfer processes, which are negligible in the dimer.

Figure 5 shows the results of our calculations for different sets of parameters. We found that smaller exciton–phonon coupling and large disorder $\lambda = 110\,\mathrm{cm}^{-1}$, $\sigma = 270\,\mathrm{cm}^{-1}$ gives the best agreement with experiment, where the peak shift decays from 25 fs at $t_2 = 0$ to a long time value of 8 fs. The difference between calculation and experiment may be reduced further by using more complex spectral densities and incorporating finite pulsewidth effects which were not included in our calculations (Yu *et al.* 1997).

(*b*) *Impulsive pump-probe spectroscopy*

We have calculated the differential absorption of a weak probe following an excitation by a very short pump. We assume that the pump pulse is shorter than the dephasing time given by the inverse of the absorption halfwidth (for the halfwidth of $315\,\mathrm{cm}^{-1}$, this requires pulses shorter than 10 fs). In this limit, the time and frequency-resolved pump-probe signal $S_{\mathrm{pp}}(\omega, t_2)$ is obtained by setting $t_1 = 0$ in equation (2.11) and performing a Fourier transform with respect to t_3:

$$S_{\mathrm{pp}}(\omega, t_2) = \mathrm{Im} \int_0^\infty \mathrm{d}t_3 \, \exp(\mathrm{i}\omega t_3) \hat{R}(t_3, t_2, 0). \tag{3.6}$$

Figure 6 shows the calculated pump-probe signal as a function of frequency ω for various values of the time delay t_2 between the pump and the probe. We used the same parameters as in the peak-shift simulations $\lambda = 110\,\mathrm{cm}^{-1}$, $\sigma = 270\,\mathrm{cm}^{-1}$. When eqsuations (2.11)–(2.14) are substituted in equation (3.6), we identify four contributions to the pump-probe signal. The window function equation (2.14) has two terms. The first term in equation (2.11) is therefore split into two contributions denoted the stimulated emission and the excited state absorption, originating from the first and the second terms of equation (2.14), respectively. The third contribution to S_{pp}, known as the bleaching term, comes from the second term in equation (2.11). Finally the forth, short-time, component is given by the third term in equation (2.11). We shall now examine these contributions separately. Figure 6*a* shows the stimulated emission (dashed line), excited state absorption (dotted line) and the bleaching contribution (solid line). The bleaching and stimulated emission result in negative differential absorption peaks, whereas the excited state absorption representing transitions from one- to two-exciton states gives a positive peak. All three contributions show extremely weak dependence on t_2 and are displayed for $t_2 = 0$. Equation (2.11) implies that the bleaching contribution does not depend on t_2 at all, whereas the weak dependence on t_2 of the other two contributions reflects the weak polaron population relaxation processes: due to selection rules the lower exciton is mainly excited

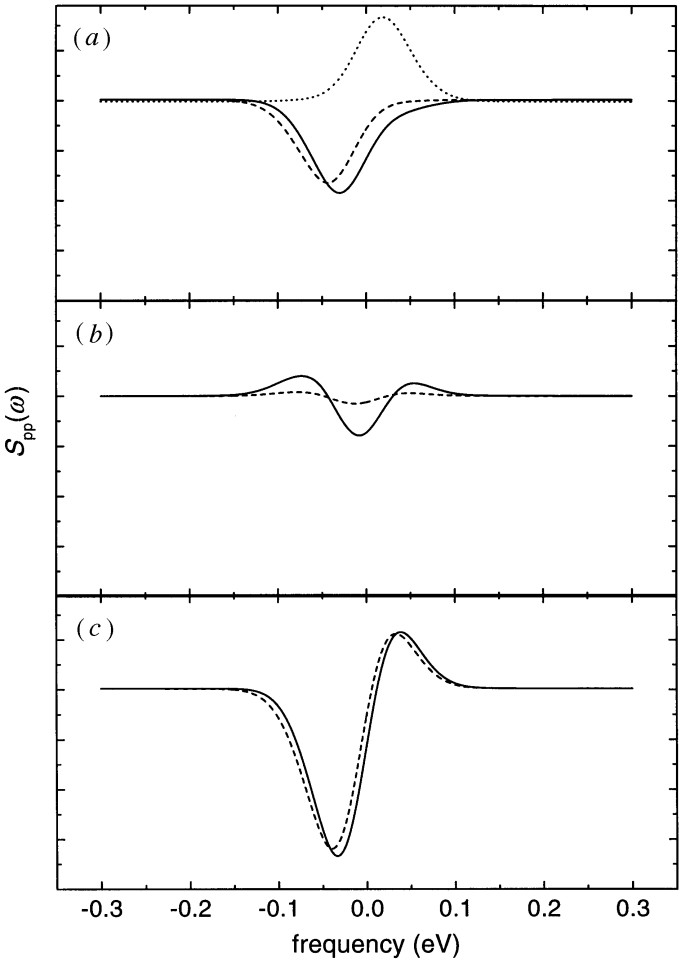

Figure 6. Pump-probe signal of the B820 dimer. $\lambda = 110\ \mathrm{cm}^{-1}$, $\sigma = 270\ \mathrm{cm}^{-1}$. (*a*) $t_2 = 0$ fs. The solid line represents bleaching contribution; dashed line, stimulated emission; and dotted line, two-exciton part of population contribution. These contributions depend weakly on t_2 and are shown for $t_2 = 0$. (*b*) The short-time contribution for two time delays. The solid line represents $t_2 = 0$ fs; dashed line, $t_2 = 200$ fs. (*c*) The total signal. The solid line represents $t_2 = 0$ fs; dashed line, $t_2 = 200$ fs.

and population relaxation does not take place. Figure 6*b* shows the fourth short-time component at $t_2 = 0$ and $t_2 = 200$ fs. The strong dependence of this component on t_2 reflects polaron formation processes. The total signal (sum of all four contributions) is given in figure 6*c* for $t_2 = 0$ and $t_2 = 200$ fs.

The arguments presented above imply that time dependence of the signal originates from the short-time component and our calculations support the following picture of relaxation in the dimer: the pump excites the lower exciton and subsequently nuclear relaxation takes place, forming the lower polaron. Polaron formation is responsible for the shift of the stimulated emission with respect to the bleaching component (nuclear Stokes shift). Electronic relaxation is negligible and the time dependence of the signal originates from nuclear relaxation in the lower excited electronic state. The more complicated relaxation mechanism in LH2 which depends on both electronic and nuclear relaxation will be studied elsewhere (Zhang *et al.* 1998).

Table 1. *Double exponential fits for numerical simulations of fluorescence depolarization in LH2*

λ (cm^{-1})	σ (cm^{-1})	r_0	τ_1 (fs)	r_1	τ_2 (fs)	r_2
320	230	0.11	23	0.17	118	0.12
240	260	0.11	31	0.17	174	0.12
160	280	0.11	44	0.17	262	0.12
80	310	0.12	70	0.15	406	0.13

4. Fluorescence depolarization of LH2

By using linearly polarized laser pulses, and setting the polarization of the incoming electric field $\boldsymbol{e}_1$ and detection $\boldsymbol{e}_s$ to be either parallel or perpendicular to each other, one can obtain the parallel component $I_\parallel$ (when $\boldsymbol{e}_s \| \boldsymbol{e}_1$) and perpendicular component $I_\perp$ (when $\boldsymbol{e}_s \perp \boldsymbol{e}_1$) of the fluorescence signal, using the formula

$$I = \sum_{\mu\nu} (\boldsymbol{e}_s \cdot \boldsymbol{d}_\mu)^2 G_{\mu\nu}(t_2)(\boldsymbol{e}_1 \cdot \boldsymbol{d}_\nu)^2. \tag{4.1}$$

The depolarization (anisotropy) signal is defined as

$$r(t) = \frac{I_\parallel(t) - I_\perp(t)}{I_\parallel(t) + 2I_\perp(t)}. \tag{4.2}$$

When the molecular orientations are distributed randomly, the ensemble average of the anisotropy should vary between $r(0) = 0.4$ and $r(\infty) = 0.1$.

Strong energetic disorder and head-to-tail dipole orientations in LH2 suggest the following depolarization mechanism. The linearly polarized pump field excites excitons localized (due to strong disorder) at two parts of the ring where dipoles are almost parallel to $\boldsymbol{e}_1$. Two types of relaxation processes then take place: nuclear relaxation which leads to the formation of polarons, and population relaxation of polarons localized at different parts of the ring which causes depolarization of the signal. Although nuclear relaxation does not lead to depolarization directly, it has an implicit influence on the process by affecting the polaron relaxation rates. The numerically calculated depolarization signal using equations (4.1) and (4.2) for various values of λ and σ are presented in figure 7 (in all cases, λ and σ are adjusted to fit the absorption linewidth). Following Jimenez *et al.* (1996), we fitted our calculated depolarization signal using a double exponential form:

$$r(t) = r_0 + r_1 \exp(-t/\tau_1) + r_2 \exp(-t/\tau_2). \tag{4.3}$$

The results of this fit are given in table 1. Table 2 summarizes the results of a double-exponential fit of experiment (Jimenez *et al.* 1997) for various values of the excitation (λ_{ex}) and detection (λ_{d}) wavelengths. A comparison of tables 1 and 2 shows that the best fit of our theory is obtained using the strongest values of energetic disorder represented by the last two lines in table 1.

5. Summary

The theory presented in this paper incorporates relaxation processes in nonlinear optical spectroscopy of molecular aggregates. The theory accounts for strong energetic disorder and exciton–phonon coupling and applies when the disorder-induced

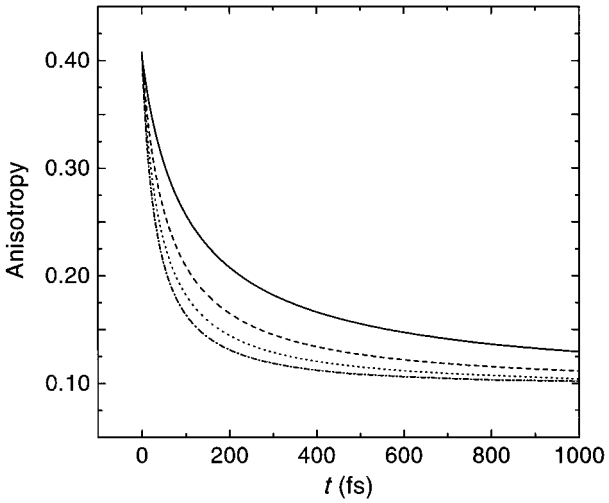

Figure 7. Fluorescence depolarization (equation 4.2) of LH2: solid line, $\lambda = 80\ \mathrm{cm}^{-1}$, $\sigma = 310\ \mathrm{cm}^{-1}$; dashed line, $\lambda = 160\ \mathrm{cm}^{-1}$, $\sigma = 280\ \mathrm{cm}^{-1}$; dotted line, $\lambda = 240\ \mathrm{cm}^{-1}$, $\sigma = 260\ \mathrm{cm}^{-1}$; dashed-dotted line, $\lambda = 320\ \mathrm{cm}^{-1}$, $\sigma = 230\ \mathrm{cm}^{-1}$.

Table 2. *Double exponential fits for fluorescence depolarization experiments in LH2 (Jimenez et al. 1996)*

$\lambda_{ex}/\lambda_{det}$ (nm)	τ_1 (fs)	r_1	τ_2 (fs)	r_2
840/940	40–50	0.2	320	0.06
850/940	82	0.18	330	0.05
860/940	90	0.21	410	0.04

exciton localization length is shorter than the phonon-induced exciton self-trapping length (polaron size) in the absence of disorder. The theory treats dynamical processes in disordered aggregates such as nuclear relaxation (formation of localized polarons) and hopping transport between polarons. Polaron transport is described by the master equation for polaron populations.

We applied the theory to calculate photon echo and pump probe signals in chlorophyll dimers and the fluorescence depolarization signal in LH2. Our calculations for the dimer show that for the impulsive pump polaron population relaxation does not affect the probe signal since the lower exciton is mainly populated by an ultrafast pump pulse, and the time-dependence of the signal only reflects polaron formation. Depolarization measurements provide a direct probe for exciton dynamics in photosynthetic complexes. Our calculations of depolarization spectroscopy in LH2 show two distinct timescales, as observed experimentally (Jimenez *et al.* 1997). The multitude of timescales can be attributed to the combined effects of fast transitions between excitons that are spatially close and slower rates between excitons that are far apart. In addition, we expect excitonic transport at short times which should turn into a slower polaron transport at longer times where the nuclear degrees of freedom have relaxed.

The support of the Air Force office of scientific research, the National Science Foundation Cen-

ter for Photoinduced Charge Transfer and the National Science Foundation through Grants no. CHE-9526125 and no. PHY94-15583 is gratefully acknowledged.

Appendix A. The short-time third-order response function

In this appendix we present expressions for the response function $R(t_3, t_2 t_1)$. By invoking the rotating wave approximation, only three contributions out of sixteen in equation (2.21) survive, the corresponding double-sided Feynman diagrams are given in figure 1. The response function adopts the form (Zhang *et al.* 1998)

$$R(t_3,t_2,t_1) = R_{\mathrm{I}}(t_3,t_2,t_1) + R_{\mathrm{II}}(t_3,t_2,t_1) + R_{\mathrm{III}}(t_3,t_2,t_1),$$

$$\begin{aligned} R_{\mathrm{I}}(t_3,t_2,t_1) = \sum_{\mu\nu} &(\boldsymbol{e}_s\cdot\boldsymbol{d}_\mu)(\boldsymbol{e}_3\cdot\boldsymbol{d}_\mu)(\boldsymbol{e}_2\cdot\boldsymbol{d}_\nu)(\boldsymbol{e}_1^*\cdot\boldsymbol{d}_\nu) \\ &\times\exp[-\mathrm{i}\epsilon_\mu(t_3+t_2)+\mathrm{i}\epsilon_\nu(t_2+t_1)] \\ &\times\exp[-F^{(1)}_{\mu\nu}(0,t_2+t_1,t_3+t_2+t_1,t_1)], \end{aligned} \tag{A 1}$$

$$\begin{aligned} R_{\mathrm{II}}(t_3,t_2,t_1) = \sum_{\mu\nu} &(\boldsymbol{e}_s\cdot\boldsymbol{d}_\mu)(\boldsymbol{e}_3\cdot\boldsymbol{d}_\mu)(\boldsymbol{e}_2\cdot\boldsymbol{d}_\nu)(\boldsymbol{e}_1^*\cdot\boldsymbol{d}_\nu)\exp[-\mathrm{i}\epsilon_\mu t_3+\mathrm{i}\epsilon_\nu t_1] \\ &\times\exp[-F^{(1)}_{\mu\nu}(0,t_1,t_3+t_2+t_1,t_2+t_1)], \end{aligned} \tag{A 2}$$

$$\begin{aligned} R_{\mathrm{III}}(t_3,t_2,t_1) = -\Bigg\{ \sum_{\mu\nu\bar{\alpha}} &(\boldsymbol{e}_s^*\cdot\boldsymbol{d}_{\mu\bar{\alpha}})(\boldsymbol{e}_3^*\cdot\boldsymbol{d}_{\nu\bar{\alpha}})(\boldsymbol{e}_2^*\cdot\boldsymbol{d}_\mu)(\boldsymbol{e}_1\cdot\boldsymbol{d}_\nu) \\ &\times\exp[-\mathrm{i}\epsilon_\mu(t_3+t_2+t_1)+\mathrm{i}\epsilon_{\bar{\nu}}t_3+\mathrm{i}\epsilon_\nu t_2] \\ &\times\exp[-F^{(2)}_{\mu\nu\bar{\alpha}}(t_1,t_2+t_1,t_3+t_2+t_1,0)]\Bigg\}^*, \end{aligned} \tag{A 3}$$

where

$$\begin{aligned} F^{(1)}_{\mu\nu}(t_4,t_3,t_2,t_1) \equiv\ & g_{\mu\mu}(t_2-t_1) - g_{\mu\nu}(t_3-t_1) + g_{\mu\nu}(t_4-t_1) \\ & + g_{\mu\nu}(t_3-t_2) - g_{\mu\nu}(t_4-t_2) + g_{\nu\nu}(t_4-t_3), \end{aligned} \tag{A 4}$$

$$\begin{aligned} F^{(2)}_{\mu\nu,\bar{\alpha}}(t_4,t_3,t_2,t_1) \equiv\ & g_{\mu\mu}(t_2-t_1) - g_{\mu\bar{\alpha}}(t_2-t_1) + g_{\mu\bar{\alpha}}(t_3-t_1) - g_{\mu\nu}(t_3-t_1) \\ & + g_{\mu\nu}(t_4-t_1) - g_{\mu\bar{\alpha}}(t_3-t_2) + g_{\mu\nu}(t_3-t_2) \\ & - g_{\mu\nu}(t_4-t_2) + g_{\bar{\alpha}\bar{\alpha}}(t_3-t_2) - g_{\bar{\alpha}\nu}(t_3-t_2) \\ & + g_{\bar{\alpha}\nu}(t_4-t_2) - g_{\bar{\alpha}\nu}(t_4-t_3) + g_{\nu\nu}(t_4-t_3). \end{aligned} \tag{A 5}$$

References

Baxter, R. 1982 *Exactly solved models in statistical mechanics*. New York: Academic.

de Boeij, W. P., Pshenichnikov, M. S. & Wiersma, D. A. 1996 *Chem. Phys. Lett.* **253**, 53.

Hoff, A. J. & Deisenhofer, J. 1997 *Phys. Rep.* **287**, 1.

Hu, X. & Schulten, K. 1997 *Phys. Today* **28** (August).

Jimenez, R., Dikshit, S. N., Bradforth, S. E. & Fleming, G. R. 1996 *J. Phys. Chem.* **100**, 6825.

Jiminez, R., van Mourik, F., Yu, J. Y. & Fleming, G. R. 1997 *J. Phys. Chem.* B **101**, 7350.

Joo, T., Jia, Y. W., Yu, J. Y., Jonas, D. M. & Fleming, G. R. 1996 *J. Phys. Chem.* **100**, 2399.

Karrasch, S., Bullough, P. A. & Ghosh, R. 1995 *EMBO J.* **14**, 631.

Koolhaas, M. H. C., van Mourik, F., van der Zwan, G. & van Grondelle, R. 1994 *J. Luminesc.* **60/61**, 515.

Meier, T., Chernyak, V. & Mukamel, S. 1997*a* *J. Chem. Phys.* **107**, 8759.

Meier, T., Chernyak, V. & Mukamel, S. 1997*b* *J. Phys. Chem.* B **101**, 7332.

Meier, T., Zhao, Y., Chernyak, V. & Mukamel, S. 1997*c* *J. Chem. Phys.* **107**, 3876.

McDermott, G., Prince, S. M., Freer, A. A., Hawthornthwaite-Lawless, A. M., Papiz, M. Z., Cogdell, R. J. & Isaacs, N. W. 1995 *Nature* **374**, 517.

Mori, H. 1965*a* *Prog. Theor. Phys.* **33**, 423.

Mori, H. 1965*b* *Prog. Theor. Phys.* **34**, 399.

Mukamel, S. 1995 *Principles of nonlinear optical spectroscopy.* Oxford University Press.

Pullerits, T. & Sundström, V. 1996 *Acc. Chem. Res.* **29**, 381.

Sundström, V. & van Grondelle, R. 1995 In *Anoxygenic photosynthetic bacteria* (ed. R. E. Blankenship, M. T. Madiga & C. E. Baner), p. 349. Dordrecht: Kluwer.

van Grondelle, R., Dekker, J. P., Gillbro, T. & Sundström, V. 1994 *Biochim. Biophys. Acta* **1187**, 1.

Yu, J. Y., Nagasawa, Y., van Grondelle, R. & Fleming, G. R. 1997 *Chem. Phys. Lett.* **280**, 404.

Zhang, W. M., Meier, T., Chernyak, V. & Mukamel, S. 1998 *J. Chem. Phys.* (In the press.)

Zwanzig, R. 1961 *Lect. Theor. Phys.* **3**, 106.

Zwanzig, R. 1964 *Physica* **30**, 1109.

PHILOSOPHICAL TRANSACTIONS OF THE ROYAL SOCIETY A MATHEMATICAL, PHYSICAL & ENGINEERING SCIENCES